Multiple Geminate Ligand Recombinations in Human Hemoglobin

Raymond M. Esquerra, Robert A. Goldbeck, Stephen H. Reaney, Abigail M. Batchelder, Youxian Wen, James W. Lewis, and David S. Kliger
Department of Chemistry and Biochemistry, University of California at Santa Cruz, Santa Cruz, California 95064 USA

ABSTRACT The geminate ligand recombination reactions of photolyzed carbonmonoxyhemoglobin were studied in a nanosecond double-excitation-pulse time-resolved absorption experiment. The second laser pulse, delayed by intervals as long as 400 ns after the first, provided a measure of the geminate kinetics by rephotolyzing ligands that have recombined during the delay time. The peak-to-trough magnitude of the Soret band photolysis difference spectrum measured as a function of the delay between excitation pulses showed that the room temperature kinetics of geminate recombination in adult human hemoglobin are best described by two exponential processes, with lifetimes of 36 and 162 ns. The relative amounts of bimolecular recombination to T- and R-state hemoglobins and the temperature dependence of the submicrosecond kinetics between 283 and 323 K are also consistent with biexponential kinetics for geminate recombination. These results are discussed in terms of two models: geminate recombination kinetics modulated by concurrent protein relaxation and heterogeneous kinetics arising from α and β chain differences.

INTRODUCTION

The ligand binding reactions of hemoglobin, the cooperative oxygen transport protein in blood, serve as a general paradigm for understanding ligand binding and allostery in proteins. Although hemoglobin dynamics are a well-developed area of biophysical investigation, molecular descriptions of ligand binding energetics and the pathway for communication between subunits remain to be fully resolved. Recent progress in defining intermediates and understanding the molecular basis of heme protein function has benefitted from the application of multichannel (Hofrichter et al., 1983), polarized absorption (Goldbeck et al., 1997; Esquerra et al., 1998b), and vibrational spectroscopies (Friedman, 1994; Jayaraman et al., 1995; Hu et al., 1996; Peterson and Friedman, 1998), giving structural and kinetic information with fast time resolution after ligand photodissociation. To the extent that the environment of the protein near the heme affects the kinetics of the geminate recombination of photolyzed ligands, studying geminate recombination in such experiments can provide further information about protein structural dynamics.

The yield of photodissociation of carbon monoxide from carbonmonoxyhemoglobin (HbCO) differs from unity as a result of geminate recombination. As much as 50% of the photolyzed hemes may recombine geminately to ligand after a nanosecond laser pulse photodissociates the CO adduct (Friedman and Lyons, 1980; Jayaraman et al., 1995). The number of ligands bound to the tetramer determines the thermodynamic equilibrium between the two canonical quaternary states, R and T. Consequently, the photolysis yield dictates how many hemoglobin molecules undergo the structural R-T transition after ligand photodissociation. The objective of many time-resolved spectroscopic investigations of hemoglobin is to describe the molecular mechanism behind the R→T structural relaxation. However, geminate recombination decreases the desired signal in such studies. Using a second pulse to rephotolyze hemes that have recombined geminately increases the number of tetramers undergoing quaternary relaxation, increasing the signal change observed. The ambiguity in excitation time introduced by rephotolyzing with a second nanosecond laser pulse is minimal in such observations because the laser delay interval can be on the order of the geminate recombination time constant, which is much smaller than the time constants associated with quaternary relaxation (Jayaraman et al., 1995; Björling et al., 1996; Goldbeck et al., 1996).

Both myoglobin and hemoglobin contain protoporphyrin IX as their prosthetic group. The observation that the geminate yield for CO recombination is at least an order of magnitude smaller in Mb (Henry et al., 1983) than in Hb (Jayaraman et al., 1995) therefore implicates the protein environment as a factor controlling the geminate kinetics. It has been demonstrated that the kinetics and yield of geminate recombination in heme proteins depend directly on both the proximal (Friedman, 1985, 1994) and distal (Petrich et al., 1994; Olson and Phillips, 1996) heme pocket protein environments. Furthermore, the structural regulation of geminate rebinding appears to vary within the distribution of conformational substates available thermally to the protein. At low temperatures (Austin et al., 1975) or in highly viscous solvents (Ansari et al., 1986; Hagen et al., 1996), where interconversion between substates is slow compared with the geminate kinetics, rebinding experiments find that the geminate recombination kinetics are represented empirically by a stretched exponential. This finding implies that the inhomogeneity in protein conformation associated with frozen conformational disorder

Received for publication 2 August 1999 and in final form 3 March 2000.
Address reprint requests to Dr. Robert A. Goldbeck, Department of Chemistry and Biochemistry, University of California, Santa Cruz, CA 95064. Tel.: 831-459-4007; Fax: 831-459-2935; E-mail: goldbeck@chemistry.ucsc.edu.

0006-3495/00/06/3227/13 $2.00

gives rise to a distribution of rebinding rate coefficients (Ansari et al., 1985; Frauenfelder et al., 1991). Rebinding becomes more exponential at higher temperatures, as thermal averaging occurs before ligand recombination.

In room temperature hemoglobin studies, geminate recombination has often been treated as a simple first-order rate process with a time constant of ~30 ns (Hofrichter et al.; 1985; Jones et al. 1992; Goldbeck et al., 1996). Nonetheless, the kinetics may be more complex if protein relaxation affects heme affinity concurrently with geminate recombination or if kinetic heterogeneity exists between chains. Moreover, the time courses of geminate recombination processes and globin structural relaxations may overlap, making differential assignments difficult. Indeed, distinguishing between protein relaxation and geminate heme-ligand recombination processes was an issue in the earliest nanosecond photolysis studies of hemoglobin (Alpert et al., 1974, 1979; Duddell et al., 1979). The double pulse experiments presented here monitor directly those hemes in which geminate recombination has occurred between laser pulses to evaluate, without interference from spectral evolutions associated with concurrent protein relaxation processes, the extent to which the room temperature geminate recombination kinetics of hemoglobin deviate from a simple exponential time course. Understanding the nature and origin of the geminate kinetics observed in these measurements is important in synthesizing the structural, spectroscopic, thermodynamic, and kinetic information into a complete molecular description of hemoglobin function.

EXPERIMENTAL

Sample preparation and instrumentation.

Hb A hemolysate, prepared as described previously (Geraci et al. 1969, Goldbeck et al., 1996), was diluted to ~120 μM (in heme) in buffer (0.1 M sodium phosphate, pH 7.3). The hemolysate contained less than 5% Hb A_2 impurity, as determined by ion exchange chromatography with a DE-52 matrix. (The results of control experiments (not shown) with purified Hb A (<1% Hb A_2) showed no significant kinetic differences from those with the unpurified hemolysate.) Placing the sample under 1 atm of CO made HbCO. Sodium dithionite added to the solution to a final concentration of 1 mM scavenged any adventitious traces of oxygen. The HbCO solution was flowed through a 0.5-mm-path-length cell under 1 atm CO and a water bath (model 1141; VWR Scientific) temperature control. The sample temperature was monitored with both a calibrated thermistor and an IR temperature probe (80T-IR; Fluke).

The instrumentation for the time-resolved absorption measurements is described elsewhere (Lewis et al., 1987), except for an additional laser providing the second photolysis pulse. Heme Soret band absorption was probed with white light from a xenon flashlamp, collimated (5-mm diameter) through the sample, focused through a 100-μm slit into a Jarrel Ash spectrograph (150 grooves/mm, 450-nm blaze grating; or 150 grooves/mm, 800-nm blaze grating), and detected with an optical multichannel analyzer (EG&G OMA II). A delay/pulse generator (Stanford Instruments DG535) controlled the timing of the detector gate and the firing of the flashlamp with respect to the second laser pulse. The delay between the second laser and the detector gate, called the gate delay, was held fixed at 300 ns. A second delay/pulse generator controlled the firing of the second laser relative to the first by applying, to an accuracy of 4 ns, a variable delay interval called the laser delay. The duration of the laser delay and the laser pulse shapes were monitored with a photomultiplier tube (Hamamatsu 3809U) and a 1.5-GHz digital oscilloscope (LeCroy 9362). The first excitation beam, polarized either vertically or horizontally, propagated at 20° with respect to the probe propagation direction. The second laser beam, vertically polarized, propagated at 45° with respect to the probe propagation direction. A polarizer placed in the probe beam before the sample was oriented at the magic angle, 54.7°, with respect to the vertical to minimize the effect of molecular rotation on the observed kinetics (Lewis and Kliger, 1991). The first 532-nm excitation pulse was produced by a frequency-doubled Quanta Ray DCR-11 Nd:YAG (5-ns FWHM) laser, and the second 532-nm excitation pulse was produced by a doubled Quanta Ray DCR-2A Nd:YAG (8-ns FWHM) laser. Both lasers delivered pulse energies of 20 mJ (10-mm diameter) to the sample with repetition rates of 2 Hz.

A saturable absorber (Strickler and Berg, 1962; Nesa et al., 1990; Yariv, 1991) consisting of rhodamine 6G in aqueous ethanol solution was used to test the effect of pulse shape on the observed kinetics of geminate recombination. The saturable absorber reduced the pulse FWHM by 1 ns and removed the pulse tail. The pulse tail intensity (5% of peak intensity without the saturable absorber, measured at 20 ns after the rise of the pulse) was reduced to undetectable levels with the absorber. The saturable absorber had no significant effect on the observed kinetics and served as a control to eliminate the possibility that rephotolysis of geminately recombined hemes by excitation energy from the tail of the laser pulse might be responsible for any observed kinetic complexity.

Data analysis

For the kinetic analysis, the absorption data (193 wavelengths ranging from 380 to 460 nm), represented as an $n \times m$ matrix, $\mathbf{A}(\lambda, t)$, were smoothed using a 15-point Savitzky-Golay algorithm and decomposed into three orthogonal matrices in a best linear least-squares representation using the method of singular value decomposition (SVD) (Golub and Reinsch, 1970; Henry and Hofrichter, 1992):

$$\mathbf{A}(\lambda, t) = \mathbf{U}(\lambda)\mathbf{S}\mathbf{V}^{\mathrm{T}}(t). \quad (1)$$

where $\mathbf{U}$ is an $n \times m$ matrix containing n orthogonal basis spectra, $\mathbf{V}^{\mathrm{T}}$ is the transpose of an $m \times m$ matrix containing the time-dependent contribution of each spectrum in $\mathbf{U}$, and $\mathbf{S}$ is an $m \times m$ diagonal matrix of the singular values of $\mathbf{A}$, which weight the contributions of the columns of $\mathbf{U}$ and $\mathbf{V}$. After SVD of spectrokinetic data, important spectral evolutions are generally associated with the largest singular values, whereas the noise tends to be associated with small values clustered over a narrow range. The data are thus filtered by retaining only the rth largest values, where r is the effective rank of the data matrix. (The rank of the Soret region spectrokinetic data measured over the entire course of photolysis and bimolecular recombination had a value of 5.)

The SVD filtered data were fitted to a sum of N exponentials,

$$\Delta\mathbf{A}(\lambda, t) = \sum_{i=1}^{N} \mathbf{b}_i(\lambda)e^{-k_i t}, \quad (2)$$

with observed rate constants equal to k_i, using a nonlinear least-squares simplex fitting procedure to give a model-independent fit of the data (Goldbeck and Kliger, 1993). The wavelength-dependent amplitude, $\mathbf{b}_i(\lambda, t)$, for each exponential lifetime is the b-spectrum for the process. The overall amplitude for each lifetime was determined by the vector norm (square root of sum of squares of elements) of its b-spectrum, normalized to the sum over b-spectra. The amplitudes measure the contribution, a combination of both spectral change and concentration, of each process to the overall spectral evolution.

For experiments measuring values determined as a function of laser delay, e.g., relative photolysis yield, the data were fitted using a nonlinear least-squares simplex algorithm (Goldbeck and Kliger, 1993). Fits to the relative photolysis yield data were constrained to relative photolysis values greater than or equal to 1. The variance between runs in these data was observed to be larger than the variance within runs, with most of the uncertainty between data sets resulting from a small normalization factor. This normalization factor reflected slight path-length variations (<5%) between experiments due to stretching and compression of the silicon sealant used to attach the quartz windows in the custom-built temperature-controlled anaerobic cells, as well as small concentration differences between experiments. Because the normalization was a systematic correction throughout a given time course measurement, the error bars in Fig. 1 were calculated after this normalization correction so as to accurately reflect the estimated standard deviation (due to nonsystematic errors) of the mean values used in the time course fitting. The zero delay time was excluded from the fits because of the 4-ns uncertainty in overlapping the excitation pulses.

RESULTS

Increase in photolysis signal due to second laser pulse

The absorption difference signal after a second excitation pulse, measured as a function of delay between lasers, reflects the extent to which photolyzed hemes geminately recombine between excitation pulses. Fig. 1 shows the relative increase in photolyzed hemes as a function of delay time, t', between the initial and final excitation pulses, along with fits to the data averaged from six sets of 64 scans. More specifically, Fig. 1 shows the relative photolysis (RP) signal measured at a fixed interval (the gate delay time, Δt) of 300 ns after the second excitation pulse, where RP is defined as

$$\mathrm{RP} = \Delta_{\mathrm{PT}}\{\Delta A(\lambda, t')\}/\Delta_{\mathrm{PT}}\{\Delta A_0(\lambda)\}. \quad (3)$$

In this expression, $\Delta_{\mathrm{PT}}\{\Delta A(\lambda,t')\}$ is the peak to trough difference of the Soret photolysis difference spectrum (measured at time Δt after the second excitation pulse) as a function of t' and $\Delta_{\mathrm{PT}}\{\Delta A_0(\lambda)\}$ is the corresponding value when the second excitation pulse is blocked from the sample ($t' = 0$). The value of RP rises from a value close to unity at zero laser delay to a limiting value of ~1.4 at $t' =$ 400 ns. The increase in RP is comparable to values typically measured for the overall geminate recombination yield of HbCO, 0.35–0.5, as expected from the analysis presented below in Eqs. 4–7. As we show below in Eqs. 4–7, these data reflect the kinetics of geminate recombination independently of any concurrent spectral relaxation effects.

The fits in Fig. 1 show that both a two-exponential fit and a stretched exponential fit better describe the laser delay dependence of RP than any single exponential fit. The lifetimes and amplitudes determined from the different fits are shown in Table 1. The first time constant in the two-exponential fit agrees well with time constants traditionally attributed to geminate recombination in hemoglobin. The two-exponential fit additionally finds a slower time constant with an amplitude that is about two-thirds of the fast component. To accommodate the long time component to the geminate recombination kinetics revealed by the RP data, the single-exponential fit found a time constant that falls between the time constants found in the two-exponential fit, although this fit is clearly much poorer than either nonexponential fit. A fit to the data with a single exponential time constant that was fixed at the conventional value, 30 ns, gave the poorest fit to the data. The improvements in fitting in going from one to two exponentials or a stretched exponential are much larger than the error bars, clearly showing that the additional parameters introduced by the nonexpo-

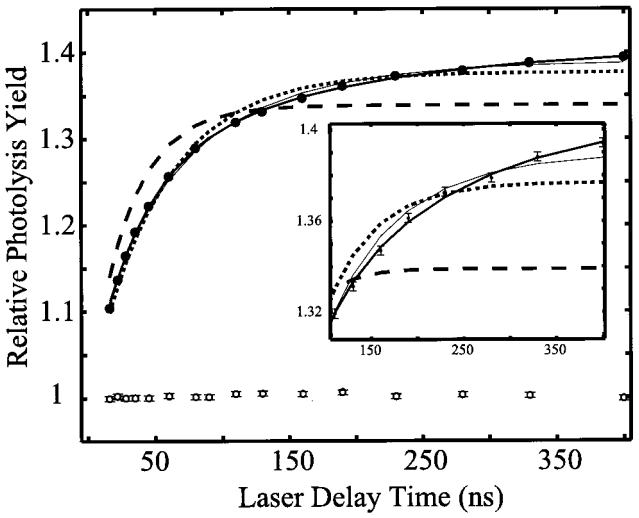

FIGURE 1 The relative photolysis (RP) signal (*filled circles*) measured 300 ns after the second of two photolysis pulses as a function of laser delay (time between first and second pulses). The RP signal is the peak-to-trough magnitude of the Soret two-pulse photolysis difference spectrum, normalized to the signal measured after a single laser photolysis pulse (second pulse blocked, laser delay = 0). The effect of rephotolysis by the second pulse is seen by comparing the two-pulse signal with the relative photolysis signal measured as a function of delay with the second laser blocked (*empty circles*). The lines represent the best least-squares fits (parameters shown in Table 1) to the RP data: two exponentials (*thick solid line*); stretched exponential (*thin solid line*); single exponential (*dotted line*); and single exponential, τ held fixed at 30 ns (*long-dashed line*). The inset shows a closer view of the RP data (and error bars) over the 125–375-ns time region, where the divergence between fits is most evident.

TABLE 1 Summary of the fits to the photolysis signal as a function of delay time between excitation pulses (τ values in nanoseconds)

	One exponential	Two exponentials*	Stretched exponential
τ_1	53 ± 6	36 ± 7 (0.63 ± 0.01)	57 ± 11
τ_2	—	162 ± 6 (0.37 ± 0.01)	—
β	—	—	0.84 ± 0.10

*Fractional amplitude values in parentheses.

nential fits are statistically justified, i.e., not simply fitting the noise.

In comparing the non-single-exponential kinetic expressions to one another, we found that the two-exponential expression fit the data significantly better than the stretched exponential expression, as shown in the inset to Fig. 1. The time constant obtained from the stretched exponential fit was close to that for the best single-exponential fit, but a β value less than unity allowed the stretched expression to better fit the long time component than did the single-exponential fit (the reduced chi-square value, χ^2_r, improved from 42 to 11). However, the four-parameter (two amplitudes, two time constants) fit using double exponentials is significantly better again than the three-parameter stretched exponential fit (χ^2_r(double-exponential) = 1.4). The F-test ratio comparing the three- and four-parameter fits is ~10, which for 12 degrees of freedom (16 time points minus 4 parameters) suggests a greater than 99% confidence in the statistical validity of adding the fourth parameter.

The relative fraction photolyzed with the second laser beam blocked from the sample is near unity for all values of t' between 0 and 400 ns, as shown in Fig. 1. This signal, which is normalized to the value at $t' = 0$, essentially measures the evolution of the peak-to-trough photolysis difference signal from 300 to 700 ns ($t' + \Delta t$) after a single photolysis pulse and provides a check for spectral relaxation effects, as discussed further below.

Extent of quaternary relaxation

Because the allosteric R-to-T transition depends on Hb ligation, the additional photolysis from the second excitation pulse correlates directly with increased T-state and decreased R-state amplitudes for bimolecular recombination of CO from the solution. Kinetic measurements of bimolecular recombination of CO from 25 μs to 40 ms (10 time points) give the relative wavelength-dependent amplitudes for bimolecular recombination to T- and R-state Hb. Under these conditions, bimolecular recombination lifetimes are ~200 μs for R and ~4 ms for T (Hofrichter et al., 1983), and the amplitudes for the processes with these lifetimes were used to determine the relative amplitude of rebinding to each state. Fig. 2 shows the relative amplitudes versus laser delay time. This gives the fraction of Hb molecules that rebind to the R and T states after rephotolysis by the second excitation pulse. Best fits from the photolysis difference rates (Table 1), with the preexponential factors determined by linear least-squares optimization, are plotted in Fig. 2. (The asymmetrical variation in amplitude for R and T rebinding is the result of convolution of amplitude associated with the $R_0 \rightarrow R_1$ subcomponent of R rebinding with a third time constant (not shown in Fig. 2) that is associated with $R_0 \rightarrow T_0$ quaternary relaxation, as discussed below.) The increased T and decreased R formation parallel the direct measurement of the photolysis signal, independently supporting the conclusion that the geminate recombination kinetics are better described by two exponentials than a single exponential.

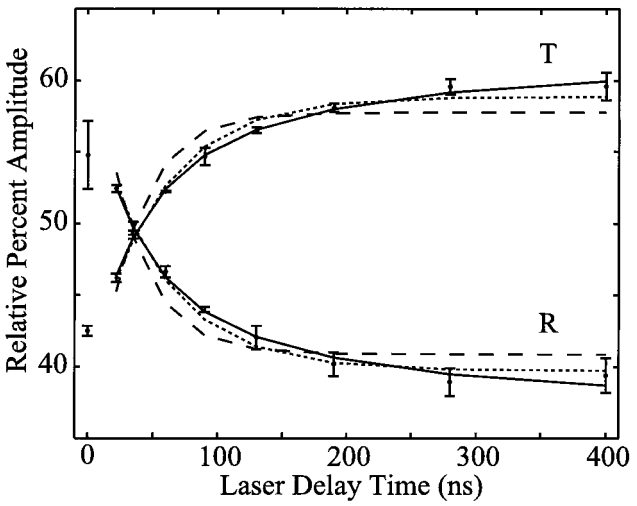

FIGURE 2 The relative percentage amplitude for bimolecular recombination to R- and T-state hemoglobin after double-pulse photolysis versus the laser delay time. The relative percentage was determined by taking the percentage of the amplitudes of the two processes from a global fit over the Soret spectral region to two exponential decays. The averaged data (*points*) and error bars from four data sets are shown, as well as fits to the following expressions, using the parameters in Table 1 and preexponential factors determined by linear least squares: two exponentials (*solid line*), best single exponential (*dotted line*), and 30-ns single exponential (*dashed line*).

Spectral evolution

The complete time course of Soret photolysis difference spectra measured from photodissociation through bimolecular recombination to reform the prephotolysis state (10 ns to 40 ms) is fit well by a sum of six exponentials (Goldbeck et al., 1996), as is the corresponding visible band evolution (R. Esquerra, unpublished results). Fig. 3 compares the normalized wavelength-dependent amplitudes (b-spectra) for the first two processes in a six-exponential fit of the visible band and the Soret time-resolved absorption data. The b-spectra for both processes primarily resemble the Hb carbonmonoxy-deoxy difference spectrum in these spectral regions, indicating a substantial spectral contribution by ligand recombination to the 100-ns process. However, small differences between the b-spectra imply that some relaxation of protein tertiary structure around the hemes is also associated with the 100-ns lifetime (although an alternative interpretation in terms of geminate spectrokinetic differences between chains is discussed below). For both bands, the first (30 ns) b-spectrum appears to be narrower and blue-shifted from the second (100 ns). Support for the presence of structural relaxation occurring concurrently with the later phase of geminate recombination also comes from time-resolved resonance Raman studies showing a

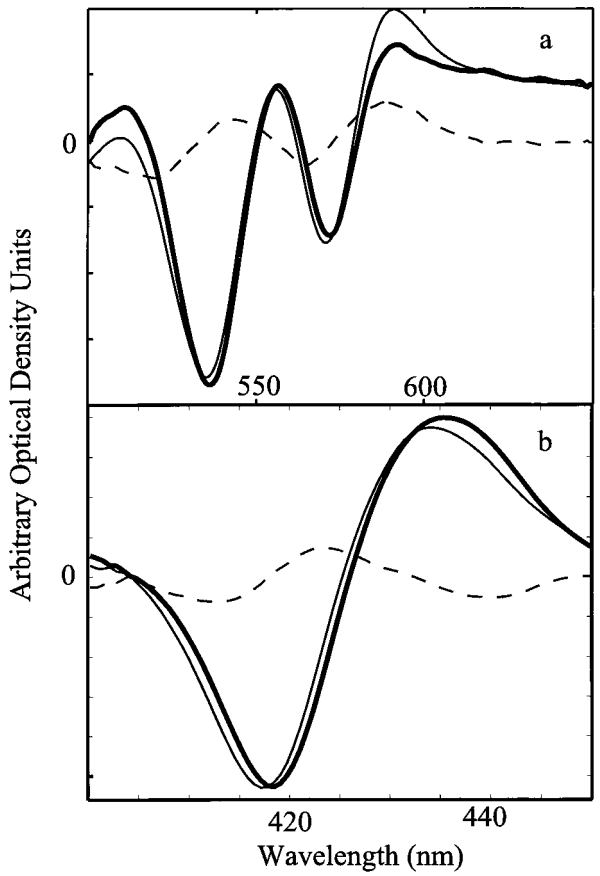

FIGURE 3 The wavelength-dependent amplitudes (b-spectra) from the first two lifetimes in a six-exponential global fit to time-resolved absorption data after photolysis of HbCO (Eq. 2). (*a*) Visible bands. (*b*) Soret. The thin line corresponds to the first b-spectrum: τ and amplitude values of 28 ns and 0.26 for the visible bands, and 29 ns and 0.28 for the Soret region. The thick line corresponds to the second b-spectrum: τ and amplitude values of 130 ns and 0.15 for the visible bands, and 110 ns and 0.18 for the Soret (see Experimental section for calculation of amplitudes). The dotted line is the difference between the first and second b-spectra, both normalized to their amplitudes.

100-ns proximal histidine bond angle relaxation process (Friedman et al., 1982; Friedman, 1994), concomitant with heme iron displacement (Spiro et al., 1990).

Temperature dependence

As the temperature is increased from 283 to 323 K, the energetic barrier to ligand escape is more readily overcome and less geminate recombination occurs (Austin et al., 1975). Early experiments by Duddell et al. (1980) observed that the Hb photolysis yield increases with temperature, from 45% at 273 K to 80% at 313 K. The geminate yield for the microsecond and nanosecond geminate phases of CO recombination in 75% glycerol solutions was shown to decrease as the temperature was raised from 220 to 300 K (Huang et al., 1997). A similar temperature dependence is observed in leghemoglobin (Stetzkowski et al., 1985), the isolated chains of Hb (Alberding et al., 1978), and the β-chains of Hb (Ansari et al., 1986).

We collected data at 10 K intervals over the range 283–323 K at 30 logarithmically spaced times from 16 ns to 20 ms (nine per decade for 16 ns to 1 μs, five per decade for 2 to 10 μs, three per decade for 10 to 100 μs, and two per decade for 200 μs to 20 ms) after a single photolysis pulse. The initial 16-ns difference spectrum increases by factors of 1.18, 1.14, 1.10, and 1.05 at increasing temperatures of 293, 303, 313, and 323 K, respectively, referenced to 283 K (data not shown). The normalized difference spectra for the 16-ns delay time at each temperature are identical, implying that the increase in signal corresponds to a decrease in geminate recombination yield in the early geminate process ($\sim$30 ns at 297 K). Fig. 4 *A* plots $\mathbf{V}_1$, the first time-dependent amplitudes of the SVD-decomposed data, normalized to the initial 16-ns time point. $\mathbf{V}_1$ generally monitors ligand recombination, and its associated basis spectrum, $\mathbf{U}_1$, closely resembles the Hb deoxy-carbonmonoxy difference spectrum (Hofrichter et al., 1983; Goldbeck et al., 1996). The plots of $\mathbf{V}_1$ show not only decreasing amplitude for the 30-ns process with increasing temperature, but also a similar decrease in the 100-ns time scale region. Significant long-term ($>$300 ns) rebinding is apparent from $\mathbf{V}_1$ at temperatures lower than 303 K. This is seen more clearly in Fig. 4 *B*, where the fractional amplitudes of both exponential phases are plotted versus temperature. The decrease in geminate amplitude observed in the $\sim$30-ns process at higher temperatures is also evident in the $\sim$100-ns process, supporting the assignment of geminate recombination as the dominant physical process contributing to the 100-ns evolution.

Photoselection

Because the rotational lifetime of hemoglobin is $\sim$30 ns (Hofrichter et al., 1991), rotation of the protein during the 8-ns FWHM excitation pulse may play a role in achieving a high degree of photolysis. Furthermore, photoselection effects from incomplete photolysis can be significant even at photolysis levels higher than 90% (Hofrichter et al., 1991). (The effect of photoselection by intense laser pulses on heme chromophores has been described in detailed by Ansari and Szabo (1993) and Ansari et al. (1993).) To ascertain the fraction of unphotolyzed hemes remaining immediately after excitation by a single pulse, the sample was excited using either a combination of two pulses with orthogonal linear polarizations or a circularly polarized pulse. A quarter-wave plate in a collinear geometry, generating circularly polarized light, will isotropically excite a sample along the probe direction (Esquerra et al., 1998a). The energy of each pulse was varied between 15 and 30 mJ for the single-pulse experiments and between 10 and 15 mJ for the double-pulse experiments. Exciting the sample with either two tempo-

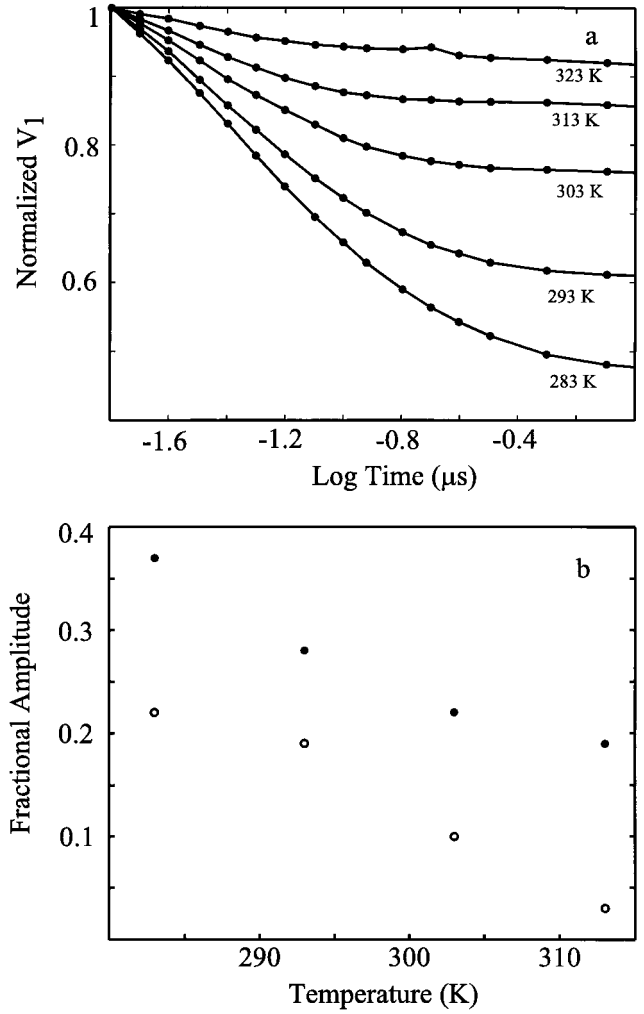

FIGURE 4 (*a*) Temperature dependence of the time-dependent amplitude, V_1, calculated from the SVD of Soret region absorption data measured from 283 to 323 K. Data are normalized to the first time point (16 ns) for comparison between temperatures. Dots represent the normalized data points; lines are linear interpolations between points. (*b*) The fractional amplitudes of the fast (●) and slow (○) geminate exponential decay components versus temperature. The amplitudes of both components decrease with temperature, as thermal promotion of ligand escape from the heme pocket lowers the yields of geminate recombination for both processes.

rally overlapped orthogonally polarized pulses or a circularly polarized pulse resulted in a 4% (±1%) increase in photolysis signal compared with a single pulse, indicating that at these laser powers ~96% of the hemes were excited in a single pulse. We thus take the value 0.96 as an estimate of the prompt photolysis yield Φ, i.e., the yield before geminate recombination. The photolysis observed at the earliest detection time, 16 ns, would actually be somewhat lower than Φ because of early geminate recombination events associated with the 30-ns process. The kinetic results were independent of the polarization of the first laser (vertical or horizontal) relative to the second, demonstrating that photoselection and rotational diffusion effects were not a significant factor in the laser time delay dependence of the double-photolysis signal at the high photolysis levels and magic angle detection used.

DISCUSSION

The photodissociation of HbCO generates up to four unligated hemes in the prompt photoproduct. Those completely deligated R-state (R_0) photoproducts that escape geminate recombination then relax to the T quaternary state rapidly enough to compete with bimolecular ligand recombination. Kinetic branching of R_0 between bimolecular recombination and quaternary relaxation forms R_1 and T_0, respectively, in roughly comparable amounts with an observed time constant of ~20 μs (although some progress along the quaternary relaxation reaction coordinate also takes place in a preceding kinetic step with a time constant of ~1 μs) (Björling et al., 1996; Goldbeck et al., 1996). The net distribution of heme ligation states after photolysis and geminate recombination is found to follow simple binomial statistics (Hofrichter et al., 1991), implying that chain differences are small and heme-heme communication is slow. A lack of difference between chains with regard to geminate recombination and an absence of intersubunit communication before ~1 μs has also been observed more directly in iron-cobalt hybrid hemoglobins (Hofrichter et al., 1985).

Within the photolysis distribution remaining after geminate recombination, the more highly ligated tetramers relax to the T state more slowly than R_0 and do not compete as effectively with diffusive ligand recombination. Thus the extent to which the aggregate sample evolves to the equilibrium T structure (before CO recombines from the solution) depends on the net photolysis yield, which in turn depends on the extent of geminate recombination. For this reason, the double-photolysis method used here can assist time-resolved spectroscopic investigations of Hb allostery by achieving an increase of as much as 40% in the number of hemes photolyzed.

$$\mathrm{HbCO} \underset{k_1}{\overset{h\nu}{\rightleftharpoons}} \mathrm{Hb_r{:}CO} \xrightarrow[-\mathrm{CO}]{k_2} \mathrm{Hb_r} \xrightarrow{k_3} \mathrm{Hb_t}$$

SCHEME 1

Scheme 1 describes the simplest view of Hb geminate recombination in which a single first-order rate process describes the geminate kinetics. The observed geminate rate is $k_{gem} = k_1 + k_2$, and the geminate recombination yield is $\phi_{gem} = k_1/(k_1 + k_2)$, where k_1 is the microscopic rate constant for the recombination of ligands that are geminately paired with heme iron by binding after photolysis to secondary sites within the heme pocket (Olson and Phillips, 1996). (The ligand is observed to move between these

secondary sites on picosecond time scales in myoglobin (Carlson et al., 1996); consequently, secondary geminate site heterogeneity is not expected to produce heterogeneity in the nanosecond kinetics of hemoglobin.) The geminate photoproduct is designated Hb_r:CO in Scheme 1 to indicate that the heme pocket is unrelaxed from the equilibrium tertiary conformation (r) found in the liganded complex. The rate constant for ligand escape from the pocket into the bulk protein solution, k_2, is much faster than the pseudo-first-order rate constant for diffusive return of the ligand to the pocket at 1 atm CO; consequently, this back-reaction is neglected in Scheme 1. Ligand escape is then followed by tertiary relaxation to the unliganded heme pocket conformation (t) with rate constant k_3. Subsequent quaternary relaxation steps leading to the T state, as well as diffusive ligand recombinations to the relaxed R and T states, are much slower and are not included in Scheme 1, which is intended only to describe the kinetics out to several hundred nanoseconds after photolysis.

The kinetics in Scheme 1 will produce two observed time constants, $\tau_1 = k_{gem}^{-1}$ (geminate recombination) and $\tau_2 = k_3^{-1}$ (tertiary relaxation). These are identified in this scenario with the first two time constants observed for HbCO, 36 and 160 ns. However, these observed constants differ by a relatively modest factor, ~4. To the extent that the time constants and associated spectral changes of these two processes overlap, it is difficult to distinguish the simple geminate behavior of Scheme 1 from more complex scenarios involving a second geminate time constant solely on the basis of analyzing absorption data for observed time constants.

In the present double-photolysis experiment, an initial laser pulse photolyzed the sample and a second pulse rephotolyzed the sample at laser delay times, t', ranging from 0 to 400 ns. The second pulse produced an increase in the overall photolysis signal as a function of t' due to the rephotolysis of hemes that have geminately recombined between pulses. The increase in relative photolysis signal is purely a population effect that reflects the geminate recombination kinetics without interference from protein relaxation effects contributing to the overall spectral dynamics measured in Soret absorption. The kinetics of geminate recombination may then be accurately determined from the t' dependence of the relative photolysis signal shown in Fig. 1. This can be seen explicitly by considering the relative photolysis signal predicted from Scheme 1,

$$RP = 1 + (1 - \Phi) + \phi_{gem}\Phi[1 - e^{-t'/\tau_1}], \qquad (4)$$

where we have assumed that Δt is long compared with τ_1 and τ_2 (see Appendix). Note the absence of spectral evolution contributed by τ_2 from this expression for the long gate delay limit used in the present measurements. A correction term for finite Δt, not shown in Eq. 4, introduces a e^{-t'/τ_2} dependence on the RP signal with an amplitude of $\delta e^{-\Delta t/\tau_2}$, where $\delta = (\Delta\Delta\epsilon_C/\Delta\Delta\epsilon_D - 1)(k_1 + k_2)/(k_1 + k_2 - k_3)$ (see Eq. A10). The magnitude of this amplitude can be evaluated from the time constants found above and an estimate of the change in Soret peak-to-trough magnitude associated with spectral relaxation. Most of the difference in peak-to-trough magnitudes, $\Delta\Delta\epsilon_C$ and $\Delta\Delta\epsilon_D$, for Hb_r and Hb_t, respectively, is expected to arise from the small (<0.5 nm) blue shift between the deoxy absorption peaks for these two species; this spectral shift accounts for the evolution of the absorption to shorter wavelength observed over the submicrosecond time scale. Given that, overall, the photolysis difference spectra for these species arise principally from the ~15-nm wavelength shift between deoxy- and carbonmonoxyHb, the change in peak-to-trough magnitude accompanying relaxation can be estimated to be less than $0.5/15 = 0.03$. Using the worst-case assumption, $\delta = 0.03/(1 - \tau_1/\tau_2)$, we estimate that the amplitude $\delta e^{-\Delta t/\tau_2}$ has a value less than 10^{-2}, more than an order of magnitude smaller than the observed biexponential amplitude. This assessment is verified by the relative photolysis signal with the second laser blocked (Fig. 1), which has the same sensitivity to $\Delta t/\tau_2$ as the double-pulse signal (Eqs. A10 and A12). The lack of observed t' dependence in the single-pulse signal demonstrates that the correction term is negligible. The nonexponential behavior shown in Fig. 1 therefore cannot be attributed simply to spectral relaxation contributions and must arise from complexity in the geminate kinetics, perhaps involving a coupling between protein relaxation and geminate rates, as discussed further below. The data presented here clearly establish that the geminate recombination kinetics cannot be described by a simple exponential time evolution and strongly suggest that a biexponential form best describes the kinetics. This kinetic form implies that either protein relaxation or heterogeneity within the tetramer affects the observed geminate recombination rates.

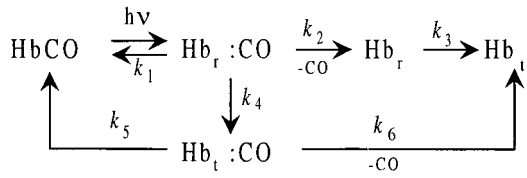

SCHEME 2

Protein relaxation concurrent with geminate recombination

Scheme 2 describes the simplest scenario for the kinetic coupling of geminate recombination with concurrent protein relaxation. The protein relaxes from Hb_r to Hb_t and the two tertiary states, having different microscopic rate constants for geminate recombination and escape, give rise to biexponential geminate kinetics. More specifically, Scheme 2 gives rise to two observed time constants for geminate recombination, $\tau_1 = (k_1 + k_2 + k_4)^{-1}$ and $\tau_2 = (k_5 + k_6)^{-1}$, corresponding to geminate recombination from Hb_r and

Hb_t, respectively. Because only two time constants are observed in the submicrosecond photolysis data, we assume that the third time constant implied by Scheme 2, $\tau_3 = k_3^{-1}$, is accidentally degenerate with τ_2 (although it is also possible that spectral similarity between Hb_r and Hb_t precludes the detection of τ_3 in the Soret absorption data). The relative photolysis signal predicted by Scheme 2 (see Appendix for explicit solutions) is

$$RP = 1 + (1 - \Phi) + \Phi a_1[1 - e^{-t'/\tau_1}] + \Phi a_2[1 - e^{-t'/\tau_2}], \quad (5)$$

where

$$a_1 = [k_1 - k_4k_5(k_1 + k_2)^{-1}](k_1 + k_2 + k_4)^{-1}, \quad (6)$$

and

$$a_2 = k_5(k_1 + k_2)^{-1}. \quad (7)$$

As in Eq. 4, these relations hold for Δt larger than τ_1 and τ_2. Equations 5–7 also assume for simplicity that $k_3 = k_4 = k_5 + k_6$, i.e., the protein relaxation rate constant is not affected by ligand escape and the relaxation time constant is roughly equal to the slower geminate time constant. This simple two-geminate-state model explains the observed biexponential Hb geminate kinetics and is consistent with spectroscopic measurements of a fast relaxation occurring in hemoglobin. Resonance Raman shows an elevated Fe-His stretching frequency (Jayaraman et al., 1995), indicating a compression of the Fe-His bond that relaxes and transfers tension to the protein coincident with geminate recombination (Jayaraman et al., 1995; Friedman et al., 1982).

The microscopic rate constants in Scheme 2 were determined from the biexponential kinetic results (Table 1) and the overall increase in RP signal (Fig. 1) by using Eqs. 6 and 7. Taking the latter value as 0.40 gives the following values for the rate constants: $k_1 = 5.7\ (\pm\ 1.0) \times 10^6\ s^{-1}$, $k_2 = 16.3\ (\pm\ 5.6) \times 10^6\ s^{-1}$, $k_3 = k_4 = 6.2\ (\pm\ 0.3) \times 10^6\ s^{-1}$, $k_5 = 5.5\ (\pm\ 1.6) \times 10^6\ s^{-1}$, and $k_6 = 0.7\ (\pm\ 1.6) \times 10^6\ s^{-1}$. These values suggest that the effect of protein relaxation on geminate recombination is almost entirely exerted through the ligand-escape rate constant, which drops by an order of magnitude ($k_6/k_2 \approx 0.04$), rather than the ligand on rate constant, which remains nearly constant. Thus the relevant tertiary relaxation in Scheme 2 is associated not so much with the decrease in the heme-proximal histidine bond angle observed in resonance Raman, which is expected to lower heme affinity, as with a change in heme pocket structure hindering ligand escape. We speculate that the hydrogen bonding of a water molecule from the bulk solvent with the distal histidine might be the 100-ns time scale (k_3^{-1}) kinetic event providing such a steric barrier to ligand escape. A water molecule hydrogen-bonded to the N_ϵ of the distal histidine is known to lower the diffusive ligand association rate constant in equilibrium deoxyMb (Carver et al., 1990; Smerdon et al., 1991). The Scheme 2 analysis does not show modulation of the geminate association rate constant, but the hydrogen-bonded water molecule is thought to lower the diffusive on rate in Mb by hindering ligand entrance to the pocket (Rohlfs et al., 1990), through the histidine gate mechanism proposed by Perutz (1989) and by steric crowding of the heme pocket. By microscopic reversibility, similar mechanisms may also lower the escape rate constant of the geminate ligand from the pocket after a water molecule enters the heme pocket and associates with the distal histidine.

One can also envision scenarios more complex than Scheme 2 that could give rise to nonexponential geminate recombination kinetics. Henry et al. (1997) modeled nonexponential relaxation in Hb, using a time-dependent rebinding rate that interpolates between geminate rebinding rate constants for two tertiary states, $k_{gem}(Hb_r)$ and $k_{gem}(Hb_t)$, according to the relation

$$k_{gem}(Hb_r/Hb_t, t) = k_{gem}(Hb_r)[k_{gem}(Hb_r)/k_{gem}(Hb_t)]^{x(t)-1}, \quad (8)$$

where $x(t)$ measures the progress of tertiary relaxation, using a stretched exponential expression,

$$x(t) = \exp\left[- \frac{(kt)^\beta}{1 + a(kt)^{\beta-1}} \right], \quad (9)$$

where the small positive constant $a = 0.001$ serves to eliminate computational singularities at $t = 0$ associated with the time derivative of an ideal stretched exponential, $e^{-(kt)^\beta}$. (Note that we have adapted the expression of Henry et al. to the present notation for the tertiary conformations.) Motivation for stretched exponential kinetics comes from low-temperature geminate recombination studies of heme proteins frozen in a glass, which show structural inhomogeneity and conformational fluctuations affecting both heme reactivity and ligand transport through the protein (Austin et al., 1975; Ansari et al., 1986; Frauenfelder et al., 1988). For a distribution of conformational substates with different geminate recombination rates, rebinding of the ensemble resembles a superposition of exponential rates when these states interconvert on time scales longer than that of geminate recombination. The kinetics are then described by a stretched exponential (Austin et al., 1975; Ansari et al., 1986; Frauenfelder et al., 1988). As discussed above, stretched exponential geminate kinetics are also expected if heme reactivity is coupled to a protein relaxation described by a stretched exponential, occurring concomitantly with geminate recombination (Hagen and Eaton, 1996; Henry et al., 1997). Nevertheless, room temperature geminate rebinding in heme proteins has generally been observed to be essentially exponential (Frauenfelder et al., 1991), indicating that the energy barriers that separate substates are sufficiently small for thermal averaging to occur on the nanosecond time scale.

Henry et al. (1997) concluded that the geminate recombination rate slows by a factor of 400 in Hb_t, compared with Hb_r. However, a comparison between that result and the

present result, showing little change in the geminate rate constant k_1, is made difficult by the very different assumptions employed in the models. The model of Henry et al. extended the equilibrium two-state model of Monod et al. (1965) to provide a comprehensive description of hemoglobin kinetics, including bimolecular recombination and tertiary and quaternary relaxation, as well as geminate recombination, using a minimum number of parameters. The simplifications used to make that model tractable included the assumptions that the geminate ligand escape rates do not depend on protein tertiary conformation and that a stretched exponential kinetic form describes the effect of tertiary relaxation on the geminate kinetics. It was also assumed that both the relaxed and unrelaxed geminate states could be treated as having identical ligand recombination and escape rate constants, with the effect of relaxation on the geminate recombination kinetics then being mimicked by varying the rate constants of both states over time, using the interpolation in Eqs. 8 and 9. Some of those a priori assumptions are addressed by the results of the present work, which suggest that ligand escape rates depend rather strongly on protein conformation and that a biexponential form is a more appropriate representation for the room temperature geminate kinetics.

$$\mathrm{Hb}_{\alpha}\mathrm{CO} \underset{k_{1\alpha}}{\overset{h\nu}{\rightleftharpoons}} \mathrm{Hb}_{\alpha,r}{:}\mathrm{CO} \xrightarrow[-\mathrm{CO}]{k_{2\alpha}} \mathrm{Hb}_{\alpha,r} \xrightarrow{k_3} \mathrm{Hb}_{\alpha,r}$$

$$\mathrm{Hb}_{\beta}\mathrm{CO} \underset{k_{1\beta}}{\overset{h\nu}{\rightleftharpoons}} \mathrm{Hb}_{\beta,r}{:}\mathrm{CO} \xrightarrow[-\mathrm{CO}]{k_{2\beta}} \mathrm{Hb}_{\beta,r} \xrightarrow{k_3} \mathrm{Hb}_{\beta,r}$$

SCHEME 3

Heterogeneous chain kinetics

Scheme 3 describes the case in which the nonexponential kinetics are attributed to chain heterogeneity within the Hb tetramer. Specifically, the observation of two geminate kinetic phases with roughly comparable amplitudes suggests that α- and β-chains within the tetramer exhibit markedly different geminate rates. The two geminate rebinding rates for the α- and β-chains are $k_{\mathrm{gem},\alpha} = k_{1\alpha} + k_{2\alpha}$ and $k_{\mathrm{gem},\beta} = k_{1\beta} + k_{2\beta}$ with corresponding yields of $\phi_\alpha = k_{1\alpha}/(k_{1\alpha} + k_{2\alpha})$ and $\phi_\beta = k_{1\beta}/(k_{1\beta} + k_{2\beta})$. The following values for the Scheme 3 microscopic rate constants were determined from the biexponential data (Table 1) by identifying $\tau_1 = k_{\mathrm{gem},\alpha}^{-1}$ and $\tau_2 = k_{\mathrm{gem},\beta}^{-1}$ on the basis of time constants observed for isolated chains (Olson et al., 1987): $k_{1\alpha} = 10.7\ (\pm\ 2.5) \times 10^6\ \mathrm{s}^{-1}$, $k_{2\alpha} = 22.6\ (\pm\ 8.0) \times 10^6\ \mathrm{s}^{-1}$, $k_{1\beta} = 3.7\ (\pm\ 0.2) \times 10^6\ \mathrm{s}^{-1}$, and $k_{2\beta} = 4.0\ (\pm\ 0.4) \times 10^6\ \mathrm{s}^{-1}$. The geminate yields are $\phi_\alpha = 0.32$ and $\phi_\beta = 0.48$. These rate constants and yields are consistent within the uncertainties with the results in Table 2 of Olson et al. (1987) for isolated chains, except for $k_{1\beta}$, which is about half of the free chain value. Although the β-chains appear to geminately recombine more slowly in the tetramer than do the α-chains, they apparently do so with a higher yield because the ligand escape rate constant is lowered more sharply in β relative to α than is the on-rate constant, as observed in independent chains.

It has been known for some time that local structure around the heme affects geminate rates (Friedman and Lyons, 1980; Rohlfs et al., 1988; Olson and Phillips, 1996). The T-state geminate rate constant is ~1000 times slower than that of the R state (Murray et al., 1988), as relaxation along the R-to-T quaternary coordinate constrains heme tertiary structure so as to hinder the in-plane movement of heme iron necessary for ligand binding at the sixth coordination site. On this basis, it would appear reasonable that differences in the heme tertiary structure for α- and β-subunits in the R-state tetramer could affect their geminate rates. It is known, for instance, that the conformations of the α- and β-chains differ in the deoxy T state (Baldwin and Chothia, 1979), leading to slightly different mechanisms for the modulation of ligand affinities. Lower oxygen affinity in the T state is achieved in the α-subunit mainly by the tilt of the proximal histidine relative to the heme plane (Perutz, 1979). For the deoxy β-subunit, obstruction by ValE11 and proximal histidine tilting combine to lower T-state oxygen affinity (Perutz, 1979). In addition to showing that isolated α- and β-chains have different apparent geminate rates and yields, Olson et al. (1971, 1987) have shown that the rate of dissociation of the fourth O_2 from Hb differs between α- and β-chains by a factor of 3, evidence of kinetic heterogeneity within the tetramer. Further evidence comes from Mathews et al. (1989), who measured a bimolecular association rate constant for CO for β that is more than a factor of 2 larger than that for the α-subunits in R-state tetrameric hemoglobin. These differences are explained by faster ligand access and exit from the β heme compared with the α heme (Olson et al., 1971; Reisberg and Olson, 1980; Mathews et al., 1989) and perhaps by a water in the distal pocket of α-chains (Mathews et al., 1989). Chain differences in tertiary configuration around the heme are also reflected in the Soret band absorption. Sugita (1974) determined that the absorption peaks of free deoxygenated α-chains are shifted to shorter wavelengths (blue shifted) from those for β-chains. The spectra of cobalt hybrids (Hofrichter et al., 1985) also show deoxy absorption peaks that are blue shifted for the α-Fe hemes compared with β-Fe hemes. Given the heterogeneity in tertiary structure and bimolecular ligand binding to the α- and β-subunits, the biexponential geminate kinetics observed in the present work may reflect different propensities to geminately rebind corresponding to different relaxed structures around the heme for each subunit. The kinetic importance of structural differences between subunits within the tetramer is also

supported by resonance Raman studies on CoHb hybrids (Friedman et al., 1982).

Most time-resolved absorption studies have ignored heterogeneity in determining Hb kinetics. A model of kinetic data incorporating a very restricted inequivalence between subunits does show a small improvement in fit compared with a model that imposes equivalence between subunits (Henry et al., 1997). A study of cobalt hybrid hemoglobins (Hofrichter et al., 1985), containing cobalt substituted into either the α or β hemes, showed different apparent geminate lifetimes (fractional amplitudes) of 76 ns (0.37) and 53 ns (0.22) for the α- and β-chains, respectively, but these differences were considered insignificant. Bandyopadhyay et al. (1992) examined the geminate rebinding of CO to Hb tetramers prepared with ligands on only the α- or β-chains and found no significant difference between the geminate rate constants for chains. It is not clear, however, how that finding compares with the present results because of the different protein conformation presented by the doubly deliganded species photolyzed in that work.

Spectral shifts implied by Schemes 2 and 3

Kinetic Scheme 3 assumes that α-chains rebind faster than β-chains, based on the observations for isolated chains (Olson et al., 1987). This leads to the prediction that the first photolysis b-spectrum will be blue shifted from the second, as observed (Fig. 3), if the first spectrum represents rebinding to the blue-shifted α-chains. Determining the spectral predictions for the protein relaxation kinetic schemes (e.g., Scheme 2), on the other hand, is not as straightforward. The static Soret absorption bands of deoxy-T Hbs are slightly blue shifted and narrowed by ~10% compared with the deoxy-R counterpart (Perutz et al., 1974). In time-resolved measurements, this blue shift is observed as a trend extending over most time scales between photolysis and bimolecular recombination (Goldbeck et al., 1996), as protein tertiary relaxation after photolysis results in an increasing blue shift of the Soret absorption of the photodissociated Hb that is thought to be correlated with an increasingly acute proximal histidine-heme plane bond angle (Perutz et al., 1974). At first sight, the b-spectra for the first two processes (time constants of 29 and 110 ns in a six-exponential fit) (Fig. 3) might not appear to follow this trend because the later spectrum is red shifted from the first, as noted above. However, the deoxy absorption shifts associated with both time constants are to shorter wavelengths, as observed in the photolysis difference spectra, because the b-spectra for the later relaxation and recombination processes are generally blue shifted from both of the early b-spectra (Goldbeck et al., 1996). (Note that b-spectra tend to represent the decay spectra of processes rather than the photolysis difference spectra of kinetic species.) Thus, if we assume that the ~100-ns time scale shift arises from protein relaxation, as in Scheme 2, then its spectral direction is consistent with the assignment of the proximal histidine bonding geometry as the relaxation coordinate affecting heme absorption. However, the trend observed in the microscopic rate constants implicated a structural change modulating ligand escape from the heme pocket rather than heme-ligand binding. Predicting the spectral shift, if any, that would accompany such a structural change requires knowing the physical nature of the relaxation, something we can only speculate about without further data. The hydrogen bonding of water to the distal histidine mentioned above in this regard could reasonably be expected to slightly shift the Soret absorption band of the adjacent heme chromophore. Direct experimental evidence for the direction of this shift appears to be lacking, but chemical intuition suggests that both increased polarity of the heme environment and weak coordination of the water molecule's oxygen atom with the heme iron would result in a red-shifted absorption for the slow geminate intermediate. This prediction would be opposite the shift to shorter wavelength absorption observed on the 100-ns time scale. It is possible, however, that spectral effects from other protein structural changes that more directly perturb heme electronic structure, such as the histidine-heme bond angle relaxation, could mask the effect of a structural relaxation modulating ligand escape located more distantly in the heme pocket.

CONCLUSIONS

By minimizing the contribution of protein relaxation to the observed kinetics, the double-photolysis method presented here measured geminate recombination more directly than a single-pulse experiment. The geminate recombination kinetics were observed to follow an extended time course that is best described by a combination of two exponential decays. Two models were considered to explain this result: 1) modulation of the heme geminate rebinding kinetics by protein relaxation and 2) kinetic heterogeneity between chains. The data presented are insufficient to definitely exclude either of these possibilities, and a combination of the two models may be needed to fully explain the complexity of geminate recombination in Hb. The chain heterogeneity model is simple, gives rate constants and yields in reasonably good agreement with the results for isolated chains, and is consistent with observed spectral shifts. However, the α, β differences in free chain geminate kinetics and tetramer bimolecular kinetics notwithstanding, there is no evidence in previous studies of metal hybrids, deliganded species, and fully liganded native Hb for significant chain differences in the geminate kinetics of the tetramer. Furthermore, the photolysis of cobalt-iron hybrids shows that the two-phase geminate kinetics observed here are also present in hybrids in which CO rebinding is restricted to either the α- or the β-chains (R. Esquerra, unpublished results). It thus seems that α, β subunit differences alone are not sufficient to account for the geminate kinetics observed

in the tetramer. This conclusion points to the need to further examine the coupling of protein relaxation and geminate rebinding discussed above as a model for the kinetic complexity observed in the tetramer. Understanding the origin of such a kinetic coupling, particularly with respect to the nature of the protein relaxation, should provide insights into how the protein modulates ligand binding and the basis of cooperativity between subunits. The microscopic rate constants from both the protein relaxation and chain heterogeneity kinetic models suggest that protein structure modulates the geminate kinetics mainly through the ligand escape rate. Further evidence about the mechanisms underlying the kinetic processes observed here may come from spectroscopic investigations using techniques, such as fast time-resolved CD and MCD, that can give more structural information about early Hb intermediates (Goldbeck et al., 1997; Esquerra et al., 1998b).

APPENDIX

Explicit kinetic solutions for Scheme 1

The Scheme 1 species are

$$A = HbCO$$

$$B = Hb_r{:}CO$$

$$C = Hb_r$$

$$D = Hb_t.$$

The time-dependent concentrations after the first photolysis pulse at $t = 0$ and a second pulse at $t = t'$ are

$$c_A(t) = (1 - \Phi)c_0 + \Phi c_0 f_A(t) + \Phi[(1 - \Phi)c_0 + \Phi c_0 f_A(t')][f_A(t - t') - 1] \quad (A1)$$

$$c_B(t) = \Phi c_0 f_B(t) + \Phi[(1 - \Phi)c_0 + \Phi c_0 f_A(t')]f_B(t - t') \quad (A2)$$

$$c_C(t) = \Phi c_0 f_C(t) + \Phi[(1 - \Phi)c_0 + \Phi c_0 f_A(t')]f_C(t - t') \quad (A3)$$

$$c_D(t) = \Phi c_0 f_D(t) + \Phi[(1 - \Phi)c_0 + \Phi c_0 f_A(t')]f_D(t - t') \quad (A4)$$

where

$$f_A(t) = k_1/(k_1 + k_2)[1 - e^{-t/\tau_1}] \quad (A5)$$

$$f_B(t) = e^{-t/\tau_1} \quad (A6)$$

$$f_C(t) = k_2/(k_1 + k_2 - k_3)[e^{-t/\tau_2} - e^{-t/\tau_1}] \quad (A7)$$

$$f_D(t) = k_2/(k_1 + k_2 - k_3) \cdot [k_3/(k_1 + k_2)\,(e^{-t/\tau_1} - 1) + 1 - e^{-t/\tau_2}], \quad (A8)$$

c_0 is the prephotolysis HbCO concentration, $\tau_1 = (k_1 + k_2)^{-1}$, $\tau_2 = k_3^{-1}$, and Φ (= 0.96) is the prompt photolysis yield, defined in the text. The relative photolysis (RP) signal measured at $t = t' + \Delta t$, where Δt = 300 ns, is

$$RP(t' + \Delta t) = \left[\sum_{i=B,C,D} \Phi c_0 \Delta_{PT}\{\Delta\varepsilon_i(\lambda)\}f_i(\Delta t)\right]^{-1} \cdot \sum_{i=B,C,D} \Delta_{PT}\{\Delta\varepsilon_i(\lambda)\}c_i(t' + \Delta t). \quad (A9)$$

In Eq. A9, $\Delta\epsilon_i(\lambda)$ is the photolysis difference extinction coefficient of species i at wavelength λ and Δ_{PT} is the peak-to-trough difference operator. If we assume that Δt is much longer than τ_1, then Eq. A9 becomes

$$RP = [1 + \delta e^{-\Delta t/\tau_2}]^{-1}[1 + (1 - \delta e^{-\Delta t/\tau_2})[(1 - \Phi) + \Phi\phi_{gem}(1 - e^{-t'/\tau_1})] + \delta e^{-(t' + \Delta t)/\tau_2}], \quad (A10)$$

where $\delta \equiv (\Delta\Delta\epsilon_C/\Delta\Delta\epsilon_D - 1)(k_1 + k_2)/(k_1 + k_2 - k_3)$, $\phi_{gem} \equiv k_1/(k_1 + k_2)$, and $\Delta\Delta\epsilon_{C,D} \equiv \Delta_{PT}\{\Delta\epsilon_{C,D}\}$. In the limit that Δt is much longer than τ_2 (or if $\Delta\Delta\epsilon_C = \Delta\Delta\epsilon_D$), Eq. A10 reduces to Eq. 4.

The relative photolysis signal with the second laser blocked is simply

$$RP_0 = \left[\sum_{i=B,C,D} \Delta_{PT}\{\Delta\varepsilon_i(\lambda)\}f_i(\Delta t)\right]^{-1} \cdot \sum_{i=B,C,D} \Delta PT\{\Delta\varepsilon_i(\lambda)\}f_i(t' + \Delta t), \quad (A11)$$

which reduces to

$$RP_0 = [1 + \delta e^{-\Delta t/\tau_2}]^{-1}[1 + \delta e^{-(t' + \Delta t)/\tau_2}] \quad (A12)$$

for Δt longer than τ_1. Note that Eqs. A10 and A12 contain the same τ_2 dependence on t'.

Explicit kinetic solutions for Scheme 2

The Scheme 2 species are

$$A = HbCO$$

$$B = Hb_r{:}CO$$

$$C = Hb_r$$

$$D = Hb_t{:}CO$$

$$E = Hb_t.$$

The time-dependent concentrations after the first photolysis pulse at $t = 0$ and a second pulse at $t = t'$ are

$$c'_A(t) = (1 - \Phi)c_0 + \Phi c_0 f'_A(t) + \Phi[(1 - \Phi)c_0 + \Phi c_0 f'_A(t')][f'_A(t - t') - 1] \quad (A13)$$

$$c'_B(t) = \Phi c_0 f'_B(t) + \Phi[(1 - \Phi)c_0 + \Phi c_0 f'_A(t')]f'_B(t - t') \quad (A14)$$

$$c'_C(t) = \Phi c_0 f'_C(t) + \Phi[(1 - \Phi)c_0 + \Phi c_0 f'_A(t')]f'_C(t - t') \quad (A15)$$

$$c'_D(t) = \Phi c_0 f'_D(t) + \Phi[(1-\Phi)c_0 + \Phi c_0 f'_A(t')] f'_D(t-t') \quad \text{(A16)}$$

$$c'_E(t) = \Phi c_0 f'_E(t) + \Phi[(1-\Phi)c_0 + \Phi c_0 f'_A(t')] f'_E(t-t'), \quad \text{(A17)}$$

where the time functions are

$$f'_A(t) = [k_1 - k_4k_5/(k_1+k_2)](k_1+k_2+k_4)^{-1}[1-e^{-t/\tau_1}] + k_4k_5(k_1+k_2)^{-1}(k_5+k_6)^{-1}[1-e^{-t/\tau_2}] \quad \text{(A18)}$$

$$f'_B(t) = e^{-t/\tau_1} \quad \text{(A19)}$$

$$f'_C(t) = k_2/(k_1+k_2)[e^{-t/\tau_2} - e^{-t/\tau_1}] \quad \text{(A20)}$$

$$f'_D(t) = k_4/(k_1+k_2)[e^{-t/\tau_2} - e^{-t/\tau_1}] \quad \text{(A21)}$$

$$f'_E(t) = [k_2 + k_4k_6/(k_5+k_6)](k_1+k_2)^{-1}[1-e^{-t/\tau_2}] + k_4(k_2+k_6)(k_1+k_2)^{-1}(k_1+k_2+k_4)^{-1} \cdot [e^{-t/\tau_1} - 1], \quad \text{(A22)}$$

and $\tau_1 = (k_1+k_2+k_4)^{-1}$, $\tau_2 = (k_5+k_6)^{-1}$. Equations A18–A22 assume that $k_3 = k_4 = k_5 + k_6$. The relative photolysis (RP) signal measured at $t = t' + \Delta t$ is

$$\mathrm{RP} = \left[\sum_{i=\mathrm{B,C,D,E}} \Phi c_0 \Delta_{PT}\{\Delta\varepsilon_i(\lambda)\} f'_i(\Delta t)\right]^{-1} \cdot \sum_{i=\mathrm{B,C,D,E}} \Delta_{PT}\{\Delta\varepsilon_i(\lambda)\} c'_i(t'+\Delta t), \quad \text{(A23)}$$

which reduces to Eq. 5 in the long Δt limit.

We thank Dr. Istvan Szundi for enlightening discussions.

We acknowledge support from the National Institutes of Health (grant GM-38549) and the National Science Foundation, Research Experiences for Undergraduates (grant CHE-9322484) for a summer fellowship for AMB.

REFERENCES

Alberding, N., S. S. Chan, L. Eisenstein, H. Frauenfelder, D. Good, I. C. Gunsalus, T. M. Nordlund, M. F. Perutz, A. H. Reynolds, and L. B. Sorensen. 1978. Binding of carbon monoxide to isolated hemoglobin chains. *Biochemistry.* 17:43–51.

Alpert, B., R. Banerjee, and L. Lindqvist. 1974. The kinetics of conformational changes in hemoglobin, studied by laser photolysis. *Proc. Natl. Acad. Sci. USA.* 71:558–562.

Alpert, B., S. El Mohsni, L. Lindqvist, and F. Tfibel. 1979. Transient effects in the nanosecond laser photolysis of carboxyhemoglobin: "cage" recombination and spectral evolution of the protein. *Chem. Phys. Lett.* 64:11–16.

Ansari, A., J. Berendzen, S. F. Bowne, H. Frauenfelder, I. E. Iben, T. B. Sauke, E. Shyamsunder, and R. D. Young. 1985. Protein states and proteinquakes. *Proc. Natl. Acad. Sci. USA.* 82:5000–5004.

Ansari, A., E. E. DiIorio, D. D. Dlott, H. Frauenfelder, I. E. Iben, P. Langer, H. Roder, T. B. Sauke, and E. Shyamsunder. 1986. Ligand binding to heme proteins: relevance of low-temperature data. *Biochemistry.* 25:3139–3146.

Ansari, A., C. M. Jones, E. R. Henry, J. Hofrichter, and W. A. Eaton. 1993. Photoselection in polarized photolysis experiments on heme proteins. *Biophys. J.* 64:852–868.

Ansari, A., and A. Szabo. 1993. Theory of photoselection by intense light pulses. Influence of reorientational dynamics and chemical kinetics on absorbance measurements. *Biophys. J.* 64:838–851.

Austin, R. H., K. W. Beeson, L. Eisenstein, H. Frauenfelder, and I. C. Gunsalus. 1975. Dynamics of ligand binding to myoglobin. *Biochemistry.* 14:5355–5373.

Baldwin, J., and C. Chothia. 1979. Haemoglobin: the structural changes related to ligand binding and its allosteric mechanism. *J. Mol. Biol.* 129:175–220.

Bandyopadhyay, D., D. Magde, T. G. Traylor, and V. S. Sharma. 1992. Quaternary structure and geminate recombination in hemoglobin: flow-flash studies on $\alpha_2{}^{CO}\beta_2$ and $\alpha_2\beta_2{}^{CO}$. *Biophys. J.* 63:673–681.

Björling, S. C., R. A. Goldbeck, S. J. Paquette, S. J. Milder, and D. S. Kliger. 1996. Allosteric intermediates in hemoglobin. 1. Nanosecond time-resolved circular dichroism spectroscopy. *Biochemistry.* 35: 8619–8627.

Carlson, M. L., R. M. Regan, and Q. H. Gibson. 1996. Distal cavity fluctuations in myoglobin: protein motion and ligand diffusion. *Biochemistry.* 35:1125–1136.

Carver, T. E., R. J. Rohlfs, J. S. Olson, Q. H. Gibson, R. S. Blackmore, B. A. Springer, and S. G. Sligar. 1990. Analysis of the kinetic barriers for ligand binding to sperm whale myoglobin using site-directed mutagenesis and laser photolysis techniques. *J. Biol. Chem.* 265: 20007–20020.

Duddell, D. A., R. J. Morris, and J. T. Richards. 1979. Ultra-fast recombination in nanosecond laser photolysis of carbonylhaemoglobin. *J. Chem. Soc. Chem. Commun.* 75–76.

Duddell, D. A., R. J. Morris, and J. T. Richards. 1980. Nanosecond laser photolysis of aqueous carbon monoxy- and oxyhaemoglobin. *Biochim. Biophys. Acta.* 621:1–8.

Esquerra, R. M., R. A. Goldbeck, D. B. Kim-Shapiro, and D. S. Kliger. 1998a. Fast time-resolved magnetic optical rotatory dispersion measurements. 1. Mueller analysis of optical and photoselection-induced artifacts. *J. Phys. Chem. A.* 102:8740–8748.

Esquerra, R. M., R. A. Goldbeck, D. B. Kim-Shapiro, and D. S. Kliger. 1998b. Spectroscopic evidence for nanosecond protein relaxation after photodissociation of myoglobin-CO. *Biochemistry.* 37:17527–17536.

Frauenfelder, H., F. Parak, and R. D. Young. 1988. Conformational substates in proteins. *Annu. Rev. Biophys. Biophys. Chem.* 17:451–479.

Frauenfelder, H., S. G. Sligar, and P. G. Wolynes. 1991. The energy landscapes and motions of proteins. *Science.* 254:1598–1603.

Friedman, J. M. 1985. Structure, dynamics, and reactivity in hemoglobin. *Science.* 228:1273–1280.

Friedman, J. M. 1994. Time-resolved resonance Raman spectroscopy as probe of structure, dynamics, and reactivity in hemoglobin. *Methods Enzymol.* 232:205–231.

Friedman, J. M., and K. B. Lyons. 1980. Transient Raman study of CO-haemoprotein photolysis: origin of the quantum yield. *Nature.* 28: 570–572.

Friedman, J. M., D. L. Rousseau, and M. R. Ondrias. 1982. Time-resolved resonance Raman studies of hemoglobin. *Annu. Rev. Phys. Chem.* 33: 471–491.

Geraci, G., L. J. Parkhurst, and Q. H. Gibson. 1969. Preparation and properties of α- and β-chains from human hemoglobin. *J. Biol. Chem.* 17:4664–4667.

Goldbeck, R. A., D. B. Kim-Shapiro, and D. S. Kliger. 1997. Fast natural and magnetic circular dichroism spectroscopy. *Annu. Rev. Phys. Chem.* 48:453–479.

Goldbeck, R. A., and D. S. Kliger. 1993. Nanosecond time-resolved absorption and polarization dichroism spectroscopies. *Methods Enzymol.* 226:147–177.

Goldbeck, R. A., S. J. Paquette, S. C. Björling, and D. S. Kliger. 1996. Allosteric intermediates in hemoglobin. 2. Kinetic modeling of HbCO photolysis. *Biochemistry.* 35:8628–8639.

Golub, G. H., and C. Reinsch. 1970. Singular value decomposition and the least squares solutions. *Numer. Math.* 14:403–420.

Hagen, S. J., and W. A. Eaton. 1996. Nonexponential structural relaxations in proteins. *J. Chem. Phys.* 104:3395–3398.

Hagen, S. J., J. Hofrichter, and W. A. Eaton. 1996. Geminate rebinding and conformational dynamics of myoglobin embedded in a glass at room temperature. *J. Phys. Chem.* 100:12008–12021.

Henry, E. R., and J. Hofrichter. 1992. Singular value decomposition: applications to experimental data. *Methods Enzymol.* 210:129–192.

Henry, E. R., C. M. Jones, J. Hofrichter, and W. A. Eaton. 1997. Can a two-state MWC allosteric model explain hemoglobin kinetics? *Biochemistry.* 36:6511–6528.

Henry, E. R., J. H. Sommer, J. Hofrichter, and W. A. Eaton. 1983. Geminate recombination of carbon monoxide to myoglobin. *J. Mol. Biol.* 166:443–451.

Hofrichter, J., E. R. Henry, J. H. Sommer, R. Deutsch, M. Ikeda-Saito, T. Yonetani, and W. A. Eaton. 1985. Nanosecond optical spectra of iron-cobalt hybrid hemoglobins: geminate recombination, conformational changes, and intersubunit communication. *Biochemistry.* 24:2667–2679.

Hofrichter, J., E. R. Henry, A. Szabo, L. P. Murray, A. Ansari, C. M. Jones, M. Coletta, G. Falcioni, M. Brunori, and W. A. Eaton. 1991. Dynamics of the quaternary conformational change in trout hemoglobin. *Biochemistry.* 30:6583–6598.

Hofrichter, J., J. H. Sommer, E. R. Henry, and W. A. Eaton. 1983. Nanosecond absorption spectroscopy of hemoglobin: elementary processes in kinetic cooperativity. *Proc. Natl. Acad. Sci. USA.* 80: 2235–2239.

Hu, X. H., H. Frei, and T. G. Spiro. 1996. Nanosecond step-scan FTIR spectroscopy of hemoglobin-ligand recombination and protein conformational changes. *Biochemistry.* 35:13001–13005.

Huang, J., A. Ridsdale, J. Wang, and J. M. Friedman. 1997. Kinetic hole burning, hole filling, and conformational relaxation in heme proteins: direct evidence for the functional significance of a hierarchy of dynamical processes. *Biochemistry.* 36:14353–14365.

Jayaraman, V., K. Rodgers, I. Mukeji, and T. Spiro. 1995. Hemoglobin allostery: resonance Raman spectroscopy of kinetic intermediates. *Science.* 269:1843–1848.

Jones, C. M., A. Ansari, E. R. Henry, G. W. Christoph, J. Hofrichter, and W. A. Eaton. 1992. Speed of intersubunit communication in proteins. *Biochemistry.* 31:6692–6702.

Lewis, J. W., and D. S. Kliger. 1991. Rotational diffusion effects on absorbance measurements: limitations to the magic-angle approach. *Photochem. Photobiol.* 54:963–968.

Lewis, J. W., G. G. Yee, and D. S. Kliger. 1987. Implementation of an optical multichannel analyzer for nanosecond flash photolysis measurements. *Rev. Sci. Instrum.* 58:939–943.

Mathews, A. J., R. J. Rohlfs, J. S. Olson, J. Tame, J. P. Renaud, and K. Nagai. 1989. The effects of E7 and E11 mutations on the kinetics of ligand binding to R state human hemoglobin. *J. Biol. Chem.* 264: 16573–16583.

Monod, J., J. Wyman, and J. P. Changeux. 1965. On the nature of allosteric transitions: a plausible model. *J. Mol. Biol.* 12:88–118.

Murray, L. P., J. Hofrichter, E. R. Henry, M. Ikeda-Saito, K. Kitagishi, T. Yonetani, and W. A. Eaton. 1988. The effect of quaternary structure on the kinetics of conformational changes and nanosecond geminate rebinding of carbon monoxide to hemoglobin. *Proc. Natl. Acad. Sci. USA.* 7:2151–2155.

Nesa, F., M. M. Martin, and Y. H. Meyer. 1990. Laser pulse shortening to subpicosecond in extracavity dye solutions. *Opt. Commun.* 75:294–300.

Olson, J. S., M. E. Andersen, and Q. H. Gibson. 1971. The dissociation of the first oxygen molecule from some mammalian oxyhemoglobins. *J. Biol. Chem.* 246:5919–5923.

Olson, J. S., and G. N. Phillips, Jr. 1996. Kinetic pathways and barriers for ligand binding to myoglobin. *J. Biol. Chem.* 271:17593–17596.

Olson, J. S., R. J. Rohlfs, and Q. H. Gibson. 1987. Ligand recombination to the alpha and beta subunits of human hemoglobin. *J. Biol. Chem.* 262:12930–12938.

Perutz, M. F. 1979. Regulation of oxygen affinity of hemoglobin: influence of structure of the globin on the heme iron. *Annu. Rev. Biochem.* 48:327–386.

Perutz, M. F. 1989. Myoglobin and haemoglobin: role of distal residues in reactions with haem ligands. *Trends Biochem. Sci.* 14:42–44.

Perutz, M. F., J. E. Ladner, S. R. Simon, and C. Ho. 1974. Influence of globin structure on the state of the heme. I. Human deoxyhemoglobin. *Biochemistry.* 13:2163–2173.

Peterson, E. S., and J. M. Friedman. 1998. A possible allosteric communication pathway identified through a resonance Raman study of four beta37 mutants of human hemoglobin A. *Biochemistry.* 37:4346–4357.

Petrich, J. W., J. C. Lambry, S. Balasubramanian, D. G. Lambright, S. G. Boxer, and J. L. Martin. 1994. Ultrafast measurements of geminate recombination of NO with site-specific mutants of human myoglobin. *J. Mol. Biol.* 238:437–444.

Reisberg, P. I., and J. S. Olson. 1980. Rates of isonitrile binding to the isolated alpha and beta subunits of human hemoglobin. *J. Biol. Chem.* 255:4151–4158.

Rohlfs, R. J., A. J. Mathews, T. E. Carver, J. S. Olson, B. A. Springer, K. D. Egeberg, and S. G. Sligar. 1990. The effects of amino acid substitution at position E7 (residue 64) on the kinetics of ligand binding to sperm whale myoglobin. *J. Biol. Chem.* 265:3168–3176.

Rohlfs, R. J., J. S. Olson, and Q. H. Gibson. 1988. A comparison of the geminate recombination kinetics of several monomeric heme proteins. *J. Biol. Chem.* 263:1803–1813.

Smerdon, S. J., G. G. Dodson, A. J. Wilkinson, Q. H. Gibson, R. S. Blackmore, T. E. Carver, and J. S. Olson. 1991. Contributions of residue 45(CD3) and heme-6-propionate to the biomolecular and geminate recombination reactions of myoglobin. *Biochemistry.* 30:6252–6260.

Spiro, T. G., G. Smulevich, and C. Su. 1990. Probing protein structure and dynamics with resonance Raman spectroscopy: cytochrome *c* peroxidase and hemoglobin. *Biochemistry.* 29:4497–4508.

Stetzkowski, F., R. Banerjee, M. C. Marden, D. K. Beece, S. F. Bowne, W. Doster, L. Eisenstein, H. Frauenfelder, L. Reinisch, E. Shyamsunder, and C. Jung. 1985. Dynamics of dioxygen and carbon monoxide binding to soybean leghemoglobin. *J. Biol. Chem.* 260:8803–8809.

Strickler, S. J., and R. A. Berg. 1962. Relationship between absorption intensity and fluorescence lifetime of molecules. *J. Chem. Phys.* 37: 814–822.

Sugita, Y. 1974. Differences in spectra of α and β chains of hemoglobin between the isolated state and in tetramer. *J. Biol. Chem.* 250: 1251–1256.

Yariv, A. 1991. Optical Electronics, 2nd Ed. Saunders College Publishers, Philadelphia. 255.